JOURNAL OF SOLID STATE CHEMISTRY 76, 284–289 (1988)

Metal–Insulator Transition in the System $(Nd_{1-x}Ca_x)MnO_{2.99}$ $(0.5 \leqq x \leqq 0.9)$

H. TAGUCHI* AND M. NAGAO

Research Laboratory for Surface Science, Faculty of Science, Okayama University, Okayama 700, Japan

AND M. SHIMADA

Department of Applied Chemistry, Faculty of Engineering, Tohoku University, Sendai 980, Japan

Received December 8, 1987; in revised form April 18, 1988

The electrical resistivity of $(Nd_{1-x}Ca_x)MnO_{2.99}$ $(0.5 \leqq x \leqq 0.9)$ was measured in the temperature range 80 to 850 K. At low temperature, all manganates are *n*-type semiconductors, and the electrical resistivity follows the Mott's $T^{-1/4}$ law, indicating the possible occurrence of variable range hopping of electrons due to Anderson localization. At high temperature, all manganates exhibit a metal–insulator transition without any crystallographic change. From the results of the magnetic susceptibility, it is concluded that the metal–insulator transition is caused by a change of the spin state of trivalent manganese ion in $(Nd_{1-x}Ca_x)MnO_{2.99}$. © 1988 Academic Press, Inc.

Introduction

In recent years, many investigations have been reported on the substitution of Ca^{2+} ion by lanthanide ions in the perovskite-type $CaMnO_3$. Jonker and Van Santen (*1*) first reported that $(La_{1-x}Ca_x)MnO_3$ was ferromagnetic in the range $0.1 \leqq x \leqq 0.5$. Wollan and Koehler (*2*) reported that $(La_{1-x}Ca_x)MnO_3$ changes from the ferromagnetic to the antiferromagnetic state at $x = 0.35$. Taguchi and Shimada (*3*) reported that $(La_{1-x}Ca_x)MnO_3$ $(0.6 \leqq x \leqq 0.95)$ exhibits *n*-type semiconducting behavior below room temperature, and the electrical resistivity follows the Mott's $T^{-1/4}$ law, indicating the possible occurrence of variable range hopping of electrons due to Anderson localization (*4, 5*) below 125 K. Above ca. 400–450 K, a metal–insulator transition occurs without a change in the crystallographic parameter.

Perovskite-type $NdMnO_3$ shows a Jahn–Teller monoclinic distortion due to the Jahn–Teller effect of the Mn^{3+} ions. The cell constants are $a = 0.5762$ nm, $b = 0.5410$ nm, $c = 0.7544$ nm, and $\beta = 89°46'$ (*6*). Bokov *et al.* (*6*) synthesized $(Nd_{1-x}Ca_x)MnO_3$ in the range $0 \leqq x \leqq 0.7$. With increasing Mn^{4+} ion content, the Jahn–Teller monoclinic distortion rapidly decreases in the range $0 \leqq x < 0.4$ and vanishes in the range $0.4 \leqq x \leqq 0.7$. From magnetic measurements, one deduces that the paramag-

* To whom all correspondence should be addressed.

0022-4596/88 $3.00

netic Curie temperature (T_θ) of $(Nd_{1-x}Ca_x)MnO_3$ increases rapidly with increasing Mn^{4+} ion content, and that the spontaneous magnetization (σ_S) of $(Nd_{1-x}Ca_x)MnO_3$ has a maximum value at $x = 0.2$.

$NdMnO_3$ is a semiconductor with the activation energy of ca. 0.25 eV; the electrical resistivity (ρ) is ca. 30 Ω cm at room temperature (*7*). There exists a "*Z*-type" jump in electrical conductivity near 1100 K; this jump corresponds to the Jahn–Teller-type crystallographic phase transition. On the other hand, $CaMnO_{3-\delta}$ is *n*-type semiconductor; log ρ below 360 K decreases with decreasing oxygen content (*8*). At low temperature, log ρ follows the Mott's $T^{-1/4}$ law (*8*), indicating a variable range hopping of electrons (*4, 5*) in this temperature range.

In the present study, the perovskite-type materials $(Nd_{1-x}Ca_x)MnO_{2.99}$ $(0.5 \leqq x \leqq 0.9)$ were synthesized in order to study the electrical transport mechanism by means of electrical resistivity and magnetic susceptibility measurements. These results provide information for the discussion of the behavior of the 3*d* electrons of Mn ions in the perkovskite-type oxide system.

Experimental

All $(Nd_{1-x}Ca_x)MnO_{3-\delta}$ $(0.5 \leqq x \leqq 0.9)$ samples were prepared using a standard ceramic technique. Powders of Nd_2O_3 (99.9%), $CaCO_3$ (99.5%), and $MnCO_3 \cdot xH_2O$ (99.4%) were weighed in the appropriate proportions and milled for 12 hr with acetone. After the mixed powders were dried at 373 K they were calcined in air at 1073 K for 24 hr, then fired at 1623 K for 24 hr under a stream of pure oxygen gas. For measuring the electrical resistivity, the powder was pressed into a pellet form under a pressure of 50 MPa, and the pellet sintered at 1623 K for 12 hr under pure oxygen. The oxygen-deficient materials obtained in this way were annealed at 873–973 K under pure oxygen for 24 hr.

The phases of the samples were identified by X-ray powder diffraction with Ni-filtered Cu$K\alpha$ radiation. The cell constants of the samples were determined from high-angle reflections using Si as a standard.

The oxygen content in each sample was determined by the oxidation-reduction (redox) method. After sodium oxalate solution and perchloric acid were added to dissolve the sample in a flask, the solution was titrated with a standard potassium permanganate solution (*9*).

The electrical resistivity was measured by a standard four-electrode technique in the temperature range 80 to 850 K. The magnetic susceptibility was measured by a magnetic torsion balance in the temperature range 80 to 700 K. The phase transition of the samples was monitored by differential thermal analysis (DTA) in the temperature range 300 to 1273 K, and by differential scanning calorimetry (DSC) below 300 K.

Results and Discussion

The oxygen content of all $(Nd_{1-x}Ca_x)MnO_{3-\delta}$ $(0.5 \leqq x \leqq 0.9)$ annealed at 873–973 K under pure oxygen was determined to be 2.99 ($\delta = 0.01$) from the chemical analysis, independent of both composition variable, x, and the annealing temperature. X-ray powder diffraction patterns of all $(Nd_{1-x}Ca_x)MnO_{2.99}$ were completely indexed as belonging to the orthorhombic perovskite-type structure. X-ray diffraction cannot detect the impurity phases below a detection limit in the order of 1–2 vol%. In the present polycrystalline samples, impurity phases may be present at or below that limit. The relation between the cell constants and the composition is shown in Fig. 1. The cell constants decreased linearly with increasing x. The ionic radius of a Ca^{2+} ion with a coordination number (CN) of 12 is 0.135 nm (*10*). Though the ionic radius of a Nd^{3+} ion with a CN of 12 is not

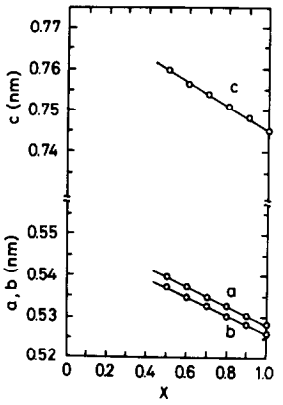

FIG. 1. Lattice parameters vs composition for the system $(Nd_{1-x}Ca_x)MnO_{2.99}$.

reported, it is extrapolated to be ca. 0.10 nm from the results of Shannon and Prewitt (*10*). The cell constants decrease linearly with increasing Ca^{2+} ion content, despite the fact that the ionic radius of Ca^{2+} is larger than that of Nd^{3+}. This linear decrease in the cell constants is explained by the increase of Mn^{4+} ion content; that is, the ionic radius of Mn^{4+} ion is smaller than that of Mn^{3+} ion located at the octahedral site (*10*).

The reciprocal temperature dependence of the electrical resistivity (ρ) in $(Nd_{1-x}Ca_x)MnO_{2.99}$ is shown in Fig. 2. Below room temperature, all $(Nd_{1-x}Ca_x)MnO_{2.99}$ ($0.5 \leqq x \leqq 0.9$) samples were *n*-type semiconductors; the electrical resistivity decreased with increasing x. With decreasing temperature, the electrical resistivity abruptly increased below ca. 250, 285, 238, and 158 K for $x = 0.5$, 0.6, 0.7, and 0.8, respectively. In this region, a plot of log ρ vs $1000/T$ was nonlinear. The transition is not very sharp due to intrinsic cationic disorder.

Analogous to the results of the electrical properties of $(Eu_{1-x}Sr_x)FeO_3$ reported by Joshi *et al.* (*4*), the plot of log ρ vs $1000/T$ is linear at high temperature, but, at low temperature, the electrical resistivity follows Mott's $T^{-1/4}$ law, indicating the possible occurrence of the variable range hopping of electrons due to Anderson localization. The relation between log ρ vs $T^{-1/4}$ in $(Nd_{1-x}Ca_x)MnO_{2.99}$ is shown in Fig. 3. As seen in Fig. 3, the log ρ vs $T^{-1/4}$ plot is linear in the temperature range 100–250 K, and log ρ strongly depends on the chemical composition. From these results, the electrical properties of $(Nd_{1-x}Ca_x)MnO_{2.99}$ can be related to the variable range hopping of electrons due to Anderson localization which was also reported for other perovskite systems such as $(Eu_{1-x}Sr_x)FeO_3$ (*4*), $CaMnO_{3-\delta}$ (*8*), and $(La_{1-x}Ca_x)MnO_3$ (*3*).

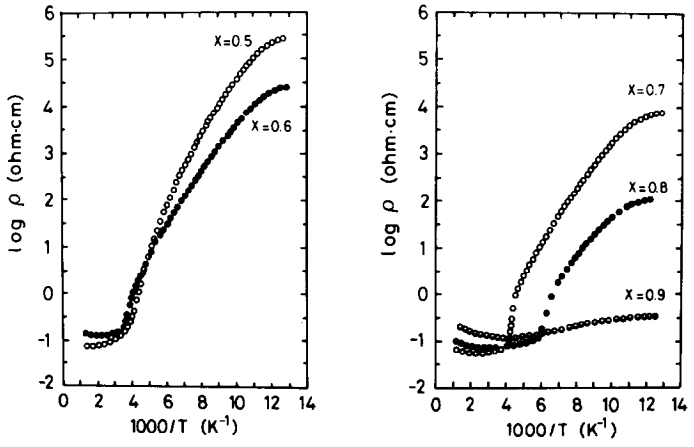

FIG. 2. Electrical resistivity vs $1/T$ for the system $(Nd_{1-x}Ca_x)MnO_{2.99}$.

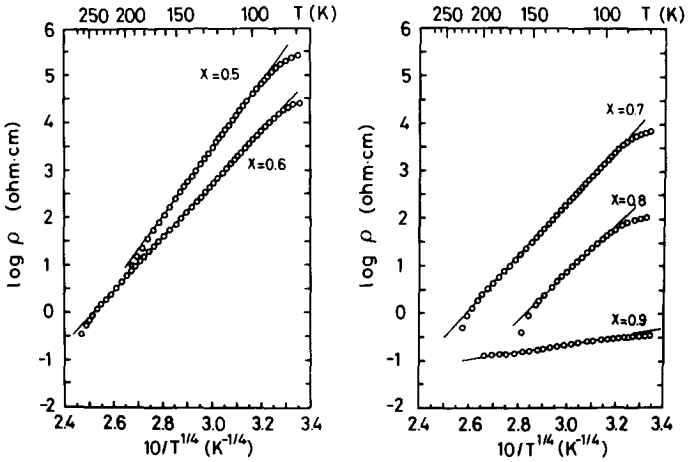

FIG. 3. Electrical resitivity vs $T^{-1/4}$ for the system $(Nd_{1-x}Ca_x)MnO_{2.99}$.

The relation between the electrical resistivity of $(Nd_{1-x}Ca_x)MnO_{2.99}$ and temperature in the range 200–1000 K is shown in Fig. 4. At high temperature, the resistivity had a positive temperature coefficient and the electrical resistivity linearly increased with increasing temperature, as shown in Fig. 4. We define the metal–insulator transition temperature (T_t) as the temperature where resistivity coefficient changes from negative to positive. The relation between T_t and the composition is shown in Fig. 5. T_t decreased strongly with increasing x. In the results of both DTA and DSC measurements on $(Nd_{1-x}Ca_x)MnO_{2.99}$, no exothermic or endothermic peaks were found close to T_t. This fact indicates that the changeover in $(Nd_{1-x}Ca_x)MnO_{2.99}$ occurs without a detectable phase transition.

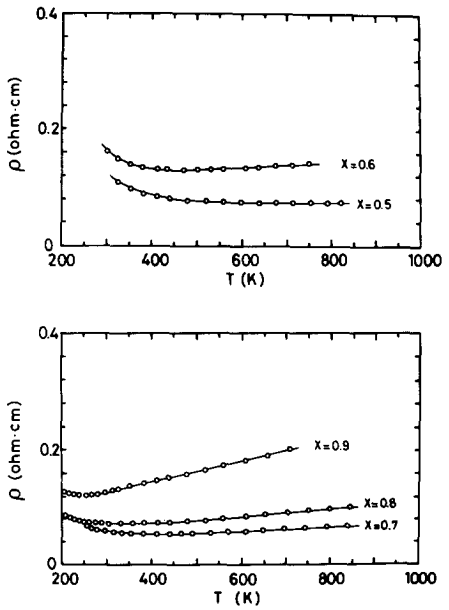

FIG. 4. Electrical resistivity vs T for the system $(Nd_{1-x}Ca_x)MnO_{2.99}$.

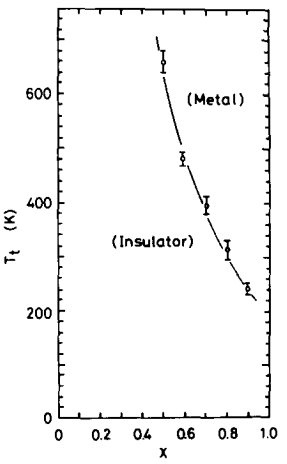

FIG. 5. Metal–insulator transition temperature vs composition for the system $(Nd_{1-x}Ca_x)MnO_{2.99}$.

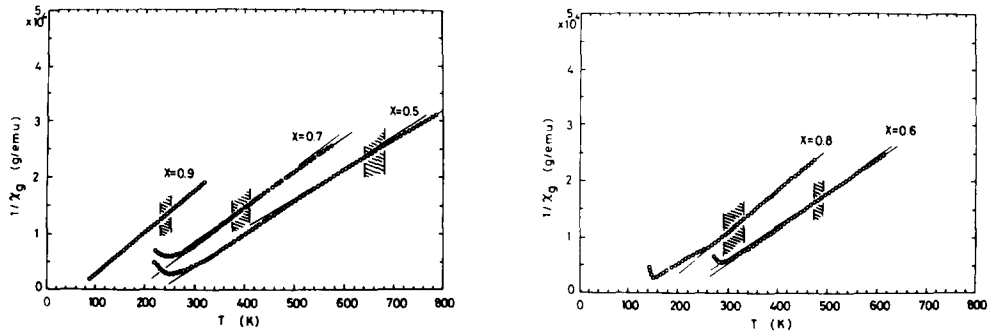

FIG. 6. Inverse magnetic susceptibility vs temperature for the system $(Nd_{1-x}Ca_x)MnO_{2.99}$.

From magnetic susceptibility measurements on $(Nd_{1-x}Ca_x)MnO_{2.99}$, positive values of paramagnetic Curie temperature (T_θ) were obtained in the composition range $0.5 \leqq x \leqq 0.8$. The temperature dependence of the inverse susceptibility ($1/\chi$) in $(Nd_{1-x}Ca_x)MnO_{2.99}$ is shown in Fig. 6. In Fig. 6, the hatchings indicate the metal–insulator transition temperature (T_t), as shown in Fig. 5. At high temperature, the $1/\chi$-T curves follow the Curie–Weiss law, and a change in slope can be seen at ca. 620, 490, 440, 280, and 230 K, for $x = 0.5$, 0.6, 0.7, 0.8, and 0.9, respectively; it is obvious that this change of slope coincides with the metal–insulator transition temperature (T_t), deduced from the resistivity measurements.

The slopes of $1/\chi$-T curves of $(Nd_{1-x}Ca_x)MnO_{2.99}$ ($0.5 \leqq x \leqq 0.7$) in the temperature range below T_t were larger than those above T_t. On the other hand, no clear changes in the slope of the $1/\chi$-T curve of $(Nd_{1-x}Ca_x)MnO_{2.99}$ ($0.8 \leqq x \leqq 0.9$) were found below and above T_t. Close to the Néel temperature (T_N), the slope of the $1/\chi$-T curve of $(Nd_{1-x}Ca_x)MnO_{2.99}$ ($0.5 \leqq x \leqq 0.7$) deviated from the Curie–Weiss law. It is believed that this deviation is caused by the residue of clusters consisting of parallel or antiparallel spins (*11*). For samples of $(Nd_{1-x}Ca_x)MnO_{2.99}$ with $0.8 \leqq x \leqq 0.9$, it is expected that the slope of the $1/\chi$-T curve would be different below and above T_t. Furthermore, the difference in temperature between T_N and T_t in $(Nd_{1-x}Ca_x)MnO_{2.99}$ with $x = 0.8$ and 0.9 is considerably smaller than that of $(Nd_{1-x}Ca_x)MnO_{2.99}$ ($0.5 \leqq x \leqq 0.7$), which might be the reason why the change in the slope of the $1/\chi$-T curve close to T_t was not found for the high x values.

The effective magnetic moment (μ_{eff}) calculated from the linear portions below and above the deflection point in the $1/\chi$-T curves are listed in Table 1. The present results suggest that a change in the electron configuration of Mn ions in $(Nd_{1-x}Ca_x)MnO_{2.99}$ affects the electrical conductivity.

An energy band scheme for perovskite-type structure was proposed by Goode-

TABLE I

THE EFFECTIVE MAGNETIC MOMENT (μ_{eff}) IN THE SYSTEM $(Nd_{1-x}Ca_x)MnO_{2.99}$

	μ_{eff} (observed)		μ_{eff} (calculated)[a]	
X	Insulator region	Metal region	Insulator region	Metal region
0.5	5.20	5.47	4.22	5.08
0.6	4.83	4.96	4.16	4.86
0.7	4.55	4.71	4.09	4.64
0.8	—	4.21	4.02	4.40
0.9	—	4.22	3.95	4.14

[a] Nd^{3+}: $\mu_{eff} = 3.5\ \mu_B$ (*13*).

nough (*12*). The band scheme consists of partially filled σ^* electron and π^* hole states. The localized π^* orbitals of α and β spins at a given cation are split by the intraatomic exchange (E_{ex}); the collective σ^* orbitals are likewise split by E_{ex}. The magnitude of the electrostatic field (Δ) depends on both the particular anion complex and the valency state of the cation. The values of μ_{eff} in $(Nd_{1-x}Ca_x)MnO_{2.99}$ change at the metal–insulator transition temperature, as shown in Table 1. The Mn^{4+} ions ($3d^3$) have the electron configuration $(d\varepsilon)^3$ $(d\gamma)^0$. On the other hand, for the Mn^{3+} ion ($3d^4$), two types of electron configurations can be proposed: One is the low-spin state $(d\varepsilon)^4$ $(d\gamma)^0$, and the other is the high-spin state, $(d\varepsilon)^3$ $(d\gamma)$. As listed in Table 1, the calculated values of μ_{eff} in $(Nd_{0.5}Ca_{0.5})MnO_{2.99}$ for the low-spin and high-spin states of Mn^{3+} ions are 4.22 and 5.08 μ_B, respectively. Although the observed values of μ_{eff} in the insulator region listed in Table 1 are larger than the calculated values, it is postulated that the low-spin state of Mn^{3+} ions partially exists below T_t, and that the spin state of Mn^{3+} ion changes from low to high above T_t. Since the electrons partially fill both collective σ^* and localized π^* orbitals, $(Nd_{1-x}Ca_x)MnO_{2.99}$ exhibits metallic behavior at temperatures above T_t.

It is concluded that $(Nd_{1-x}Ca_x)MnO_{2.99}$ $(0.5 \leqq x \leqq 0.9)$ exhibits the metal–insulator transition without a detectable phase transition at high temperature. The value of μ_{eff} changes in the neighborhood of the metal–insulator transition temperature (T_t), and the electrical properties are influenced by the electron configuration of the Mn ion.

Acknowledgments

The authors express their thanks to Professor S. Kume of Osaka University for DSC measurements and Dr. H. Kido of Osaka Municipal Technical Research Institute for the magnetic measurements.

References

1. G. H. Jonker and J. H. Van Santen, *Physica* **16,** 337 (1950).
2. E. O. Wollan and W. C. Koehler, *Phys. Rev.* **100,** 545 (1955).
3. H. Taguchi and M. Shimada, *J. Solid State Chem.* **62,** 290 (1986).
4. V. Joshi, O. Parkash, G. N. Rao, and C. N. R. Rao, *J. Chem. Soc., Faraday Trans. 2* **75,** 1199 (1979).
5. N. F. Mott, *Adv. Phys.* **21,** 785 (1972).
6. V. A. Bokov, N. A. Grigoryan, M. F. Bryzhina, and V. V. Tikhonov, *Phys. Status Solidi* **28,** 835 (1968).
7. N. Kamegashira and Y. Miyazaki, *Phys. Status Solidi A* **76,** K39 (1983).
8. K. Taguchi, *Phys. Status Solidi A* **88,** K79 (1985).
9. N. Mizutani, N. Okauma, A. Kitazawa, and M. Kato, *Kogyo Kagaku Zasshi* **73,** 1103 (1970).
10. R. D. Shannon and C. T. Prewitt, *Acta Crystallogr. Sec. B* **25,** 925 (1969).
11. S. Chikazumi, "Physics of Ferromagnetism," Vol. 1, p. 136, Syokabo Publ., Tokyo (1979). [In Japanese]
12. J. B. Goodenough, *J. Appl. Phys.* **37,** 1415 (1966).
13. T. Shin-ike, T. Sakai, G. Adachi, and J. Shiokawa, *Mater. Res. Bull.* **12,** 831 (1977).